Supporting Information

for

Hollow PtCu nanorings with high performance for methanol oxidation reaction and their enhanced durability by trace Ir

Yan Shi[a], *Yan Fang*[a], *Genlei Zhang* [a, b, *], *Xianshun Wang*[a], *Peng Cui*[a], *Qi Wang* [a], *Yuxin Wang* [c]

[a] *Anhui Province Key Laboratory of Advanced Catalytic Materials and Reaction Engineering, Anhui Province Key Laboratory of Controllable Chemistry Reaction and Material Chemical Engineering, School of Chemistry and Chemical Engineering, Hefei University of Technology, Hefei, 230009, PR China*

[b] *School of Materials Science and Engineering, Hefei University of Technology, Tunxi Road 193, Hefei, 230009, PR China*

[c] *School of Chemical Engineering and Technology, Tianjin University, Tianjin, 300350, PR China*

Corresponding Author

*E-mail: genleizhang@hfut.edu.cn

Number of pages: 37

Number of figures: 25

Number of tables: 6

Note: The figures, tables and text in this Supporting Information document are presented in the order in which they are referenced in the main paper.

Experimental section

Materials

Platinum acetylacetonate ($Pt(acac)_2$), copper acetylacetonate ($Cu(acac)_2$), iridium acetylacetonate ($Ir(acac)_3$), cetyltrimethylammonium chloride (CTAC), hexadecyltrimethylammonium bromide (CTAB), glucose, ascorbic acid (AA), and oleylamine (OAm), ethanol, methanol, sulfuric acid and other chemical reagents were purchased from Sinopharm Chemical Reagent Co. Ltd., China. Poly(vinylpyrrolidone) (PVP, MW≈55000) was purchased from Sigma-Aldrich. Carbon black (Vulcan XC-72), commercial carbon supported Pt-Ru catalyst from Johnson Matthey (PtRu/C-JM, Pt and Ru loadings in this catalyst are 20 % and 10 % in theory, respectively) and Nafion solution (5 wt%) were purchased from Hesen electric Co. Ltd., China. All aqueous solutions were prepared using deionized (DI) water. High purity nitrogen (≥ 99.99%) was supplied by Nanjing Special Gas Factory Co., Ltd., China. Glassy carbon electrode ($0.071 cm^2$ in area) was purchased from Tianjin Aida Tech. Co. Ltd., China.

Preparation of *s*-$Pt_{0.75}Cu$ nanocrystals

Typically, 10.0 mg of $Pt(acac)_2$, 9.0 mg of $Cu(acac)_2$, 5.0 mL of benzyl ether, 1.0 mL OAm and 0.5 mL oleic acid were mixed in a three-neck flask and heated to 120 ◦C for 20 min under an Ar stream. The mixture solution was heated from room temperature to 160 ºC in 20 min and kept at 160 ºC for 1 hour in a vacuum oven before it was cooled to room temperature. The resulting product was collected by repeated centrifugation and washed several times with an ethanol/cyclohexane mixture and the obtained *s*-$Pt_{0.75}Cu$ NCs were stored in cyclohexane.

Preparation of carbon-supported PtCu catalysts

Typically, the obtained $Pt_{0.75}Cu$ NRs (10 mg in 5 mL cyclohexane) were mixed with carbon black (XC-72, 40 mg) suspended in cyclohexane (10 mL). The mixture was ultrasonicated for 1 h and kept stirring at room temperature overnight. Finally, the *r*-$Pt_{0.75}Cu/C$ catalyst was separated by centrifugation, washed five times with ethanol/cyclohexane mixture, and re-dispersed in ethanol for electro-catalytic tests. As for $Pt_{0.5}Cu$, Pt_1Cu, *s*-$Pt_{0.75}Cu$ nanostructures and Ir-doped $Pt_{0.75}Cu$ NRs, the experimental procedure was the same as above, and the $Pt_{0.5}Cu/C$, *r*-Pt_1Cu/C, *s*-$Pt_{0.75}Cu/C$ and *r*-$Pt_{0.75}Ir_xCu/C$ (x = 0.02, 0.05 and 0.1) catalysts were obtained, respectively. The Pt weight contents for all catalysts were determined by ICP-AES and the results were displayed in **Table S1**.

Characterizations

Transmission electron microscopy (TEM) and high-resolution TEM (HRTEM) were performed using JEOL 2100F microscope (JEOL; Japan) operated at 200 kV. Energy dispersive X-ray spectroscopy (EDS) analysis and high-angle annular dark-field scanning TEM (HAADF-STEM) were also conducted using the same instrument to identify the elemental composition of the products. All the samples for TEM study were prepared by dropping an ethanol diluted suspension of the catalyst onto a copper grid coated with carbon film. The X-ray diffraction (XRD) spectra were conducted via a Rigaku D/Max-2500 X-ray diffractometer (Rigaku; Japan) with a Cu K_α source recorded. Raman spectra were recorded using a Renishaw 2000 system with an argon ion laser (514.5 nm) and a charge-coupled device detector. The X-ray photoelectron spectroscopy (XPS) data were collected using PHI-5000 versa probe (Ulvac-Phi; Japan) with an Al K_α source. All the spectra were corrected using C 1s signal located at 284.5 eV. Deconvolution of the spectra was carried out using the software XPS Peak 4.1 with thoroughly considering the constraints on binding energy, peak area and full width at half maximum. Metal contents in all catalysts were determined by the inductively coupled plasma atomic emission spectroscopy (TJA RADIAL IRIS 1000 ICP-AES).

Electrochemical measurements

The electrochemical measurements were conducted via a PARSTAT 2273 electrochemical workstation at room temperature. A three-electrode system which was composed of a glassy carbon electrode as the working electrode ($0.071 cm^2$ geometric area), a Pt sheet (2×2 cm^2) as counter electrode and a saturated KCl Hg/$HgCl_2$ as reference electrode was employed for the electrochemical test. Typically, the as-prepared catalyst (2.0 mg) and Nafion solution (30 μL, 5.0 wt %) were dissolved in an ethanol aqueous (1 mL, $V_{ethanol}/V_{water}$ = 1/4) and then sonicated for 30 min to form a catalyst ink. Next, 3.0 μL of the catalyst ink was dropped onto the polished working electrode and dried in an oven at 60 ºC for about 20 min. The metal mass was obtained from the total amount of catalyst on the electrode and the composition of the catalyst determined by ICP-AES. Subsequently, the working electrode covered with catalyst was activated in a N_2-saturated 0.5 M H_2SO_4 solution via cyclic voltammetry (CV) between -0.2 V and 1.1 V at a scan rate of 20 mV s^{-1} until it approached to a steady state. The electrochemically active surface area (ECSA) of a catalyst can calculated by measuring the charge collected in the hydrogen adsorption/desorption region after double-layer correction and assuming a value of 210 uC cm^{-2} for the adsorption of a hydrogen monolayer under acid medium.

The methanol electrooxidation was carried out in a N_2-saturated aqueous solution containing 0.5 M H_2SO_4 and 1.0 M methanol also between -0.2 V and 1.1 V at a scan rate of 20 $mV{\cdot}s^{-1}$. Chronoamperometry (CA) tests were carried out at 0.6 V (*vs*. SCE) for a period of 3600 s. The long-term durability of the catalysts was carried out in a N_2-saturated aqueous solution containing 0.5 M H_2SO_4 and 1.0 M methanol by a continuous 500, 2000 and 10000 potential cycles between -0.2 V and 1.1 V at a scan rate of 20 $mV{\cdot}s^{-1}$.

Supporting Figures

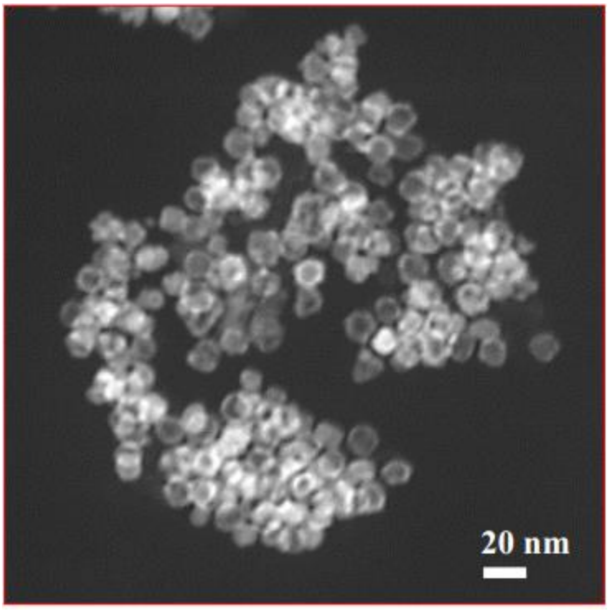

Fig. S1 HAADF-STEM image of the $Pt_{0.75}Cu$ NRs.

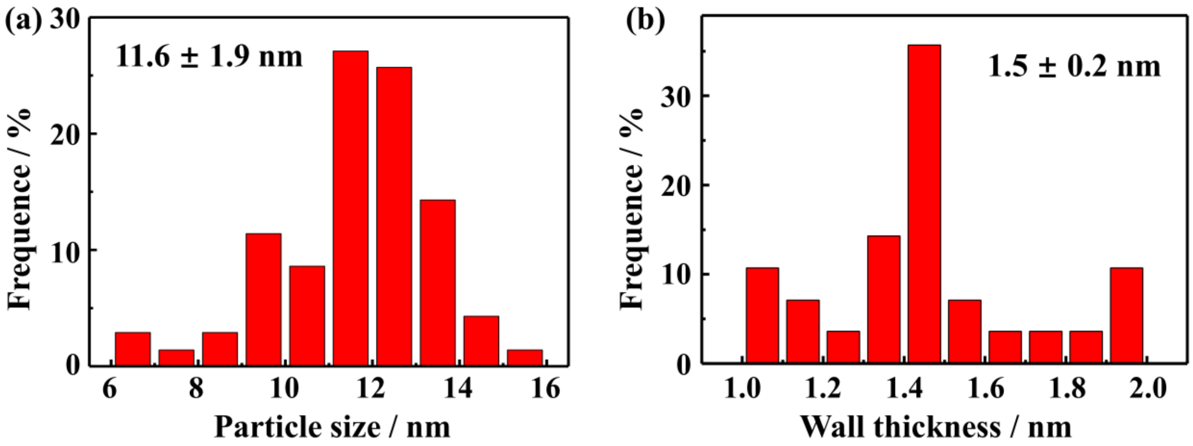

Fig. S2 (a) Particle size and (b) ring wall thickness histograms of the $Pt_{0.75}Cu$ NRs.

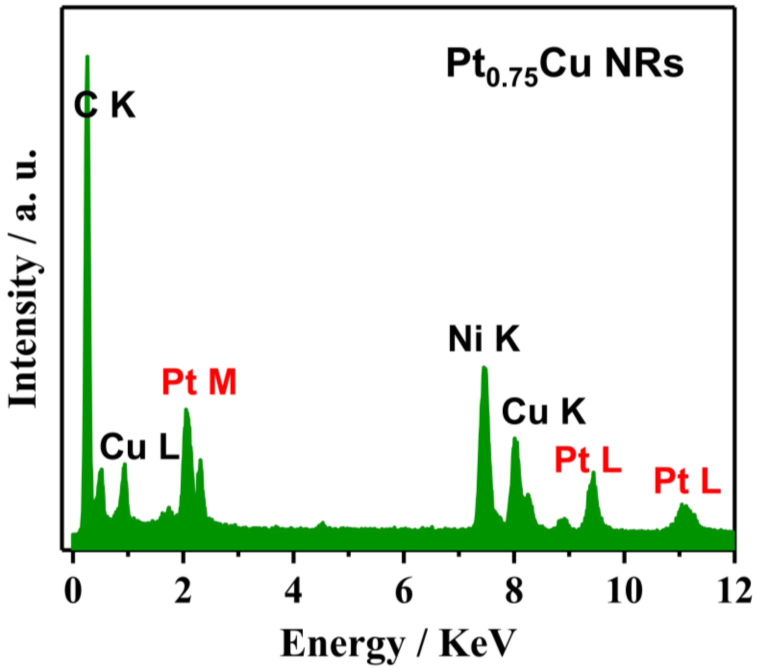

Fig. S3 The EDS spectrum of the Pt$_{0.75}$Cu NRs. The additional Ni signal arises from the nickel TEM grid.

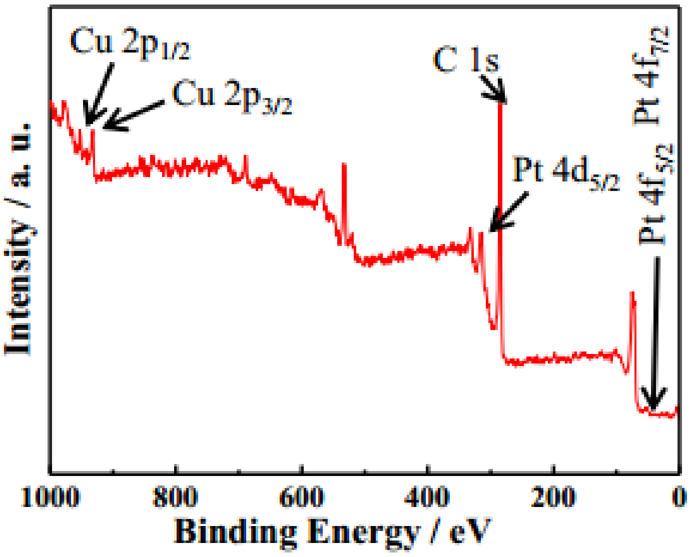

Fig. S4 The XPS survey spectrum of the $Pt_{0.75}Cu$ NRs.

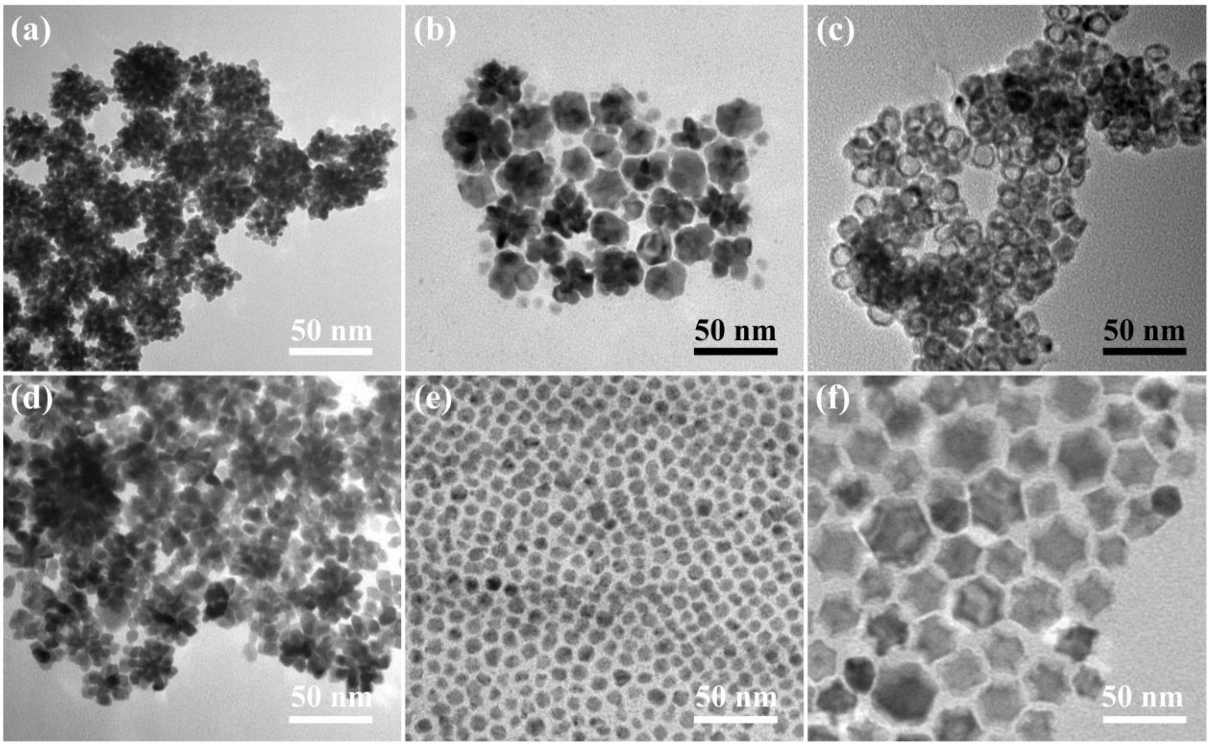

Fig. S5 The TEM images of the products with the same reaction conditions as those of $Pt_{0.75}Cu$ NRs but in the absence of (a) both glucose and CTAC, (b) CTAC; changing CTAC with (c) CTAB and (d) NH_4Cl; (e) in the absence of glucose; (f) changing glucose with AA.

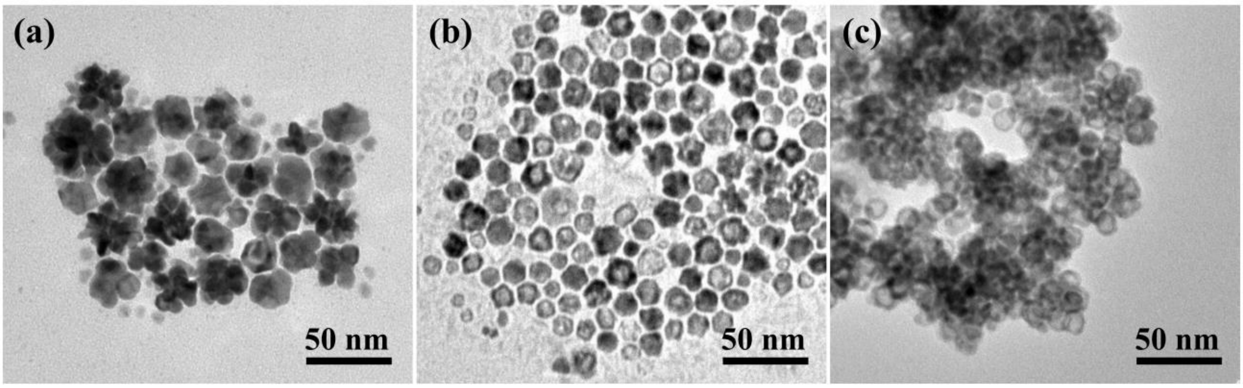

Fig. S6 The TEM images of the products with the same reaction conditions as those of $Pt_{0.75}Cu$ NRs except the use of (a) 0 mg CTAC, (b) 16 mg CTAC and (c) 48 mg CTAC.

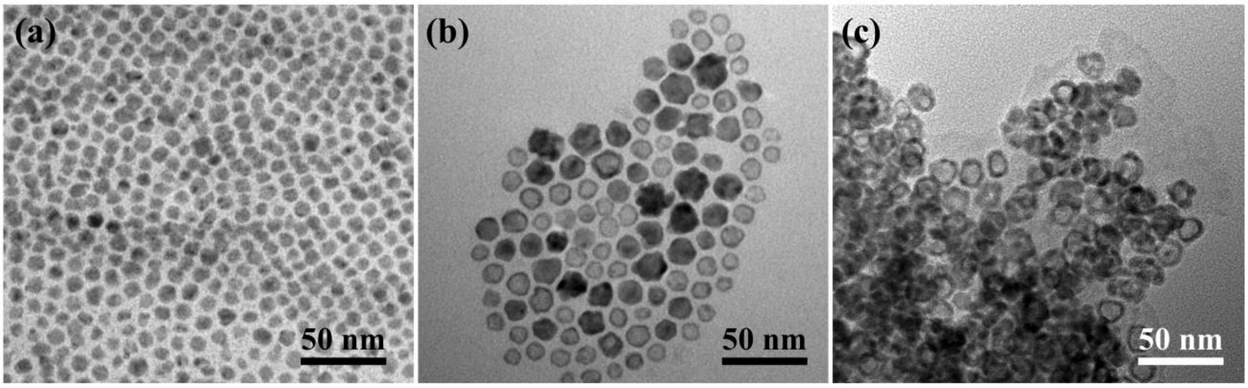

Fig. S7 The TEM images of the products with the same reaction conditions as those of $Pt_{0.75}Cu$ NRs except the use different amounts of glucose: (a) 0 mg, (b) 30 mg and (c) 90 mg.

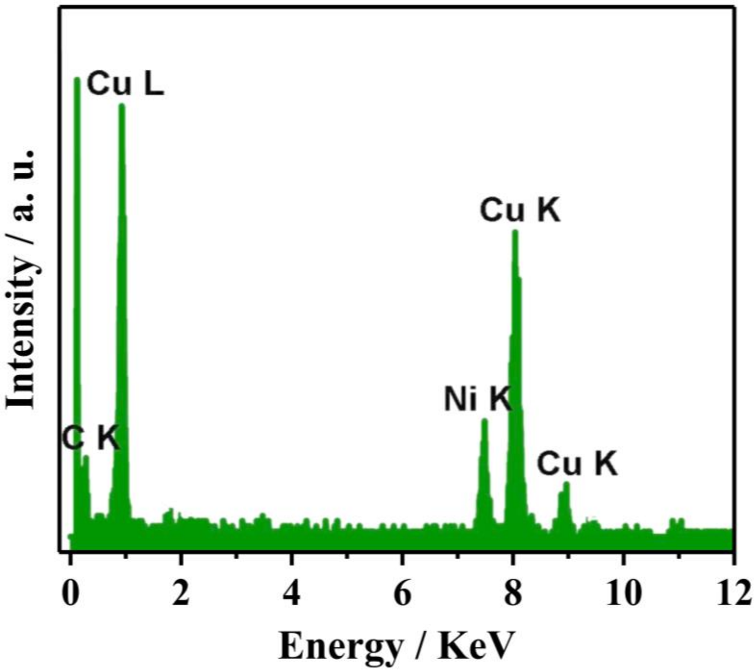

Fig. S8 The EDS spectrum of the intermediate product synthesized at the reaction time of 0.5 h. The additional Ni signal arises from the nickel TEM grid.

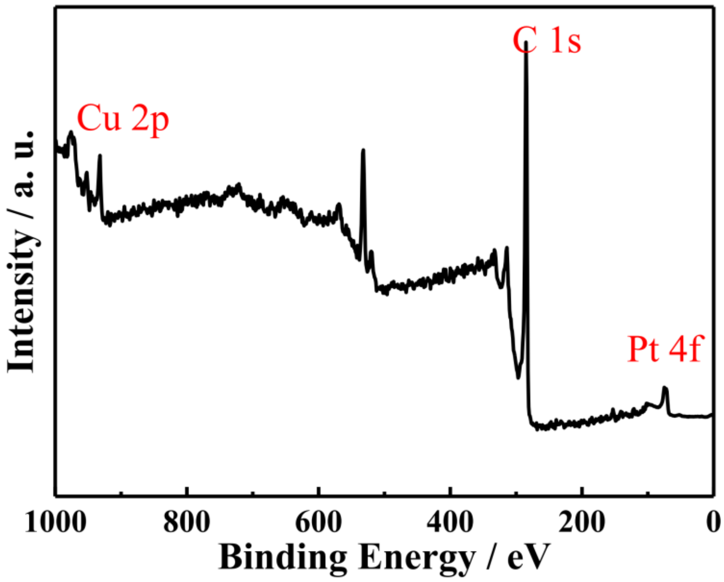

Fig. S9 The XPS survey spectrum of the intermediate product synthesized at the reaction time of 1 h.

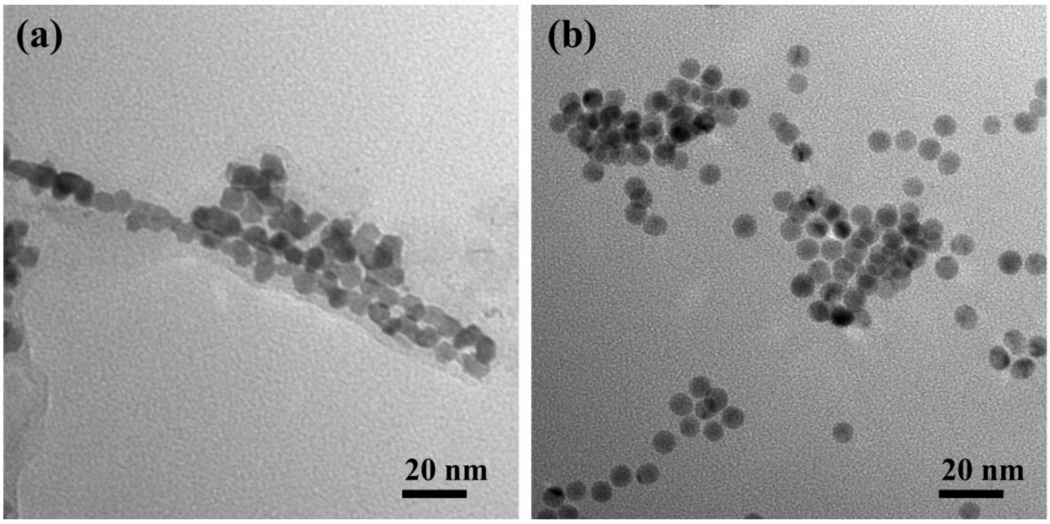

Fig. S10 Representative TEM images of the products collected from the reaction with the same condition used in the synthesis of $Pt_{0.75}Cu$ NRs but in the absent of (a) $Cu(acac)_2$ and (b) $Pt(acac)_2$.

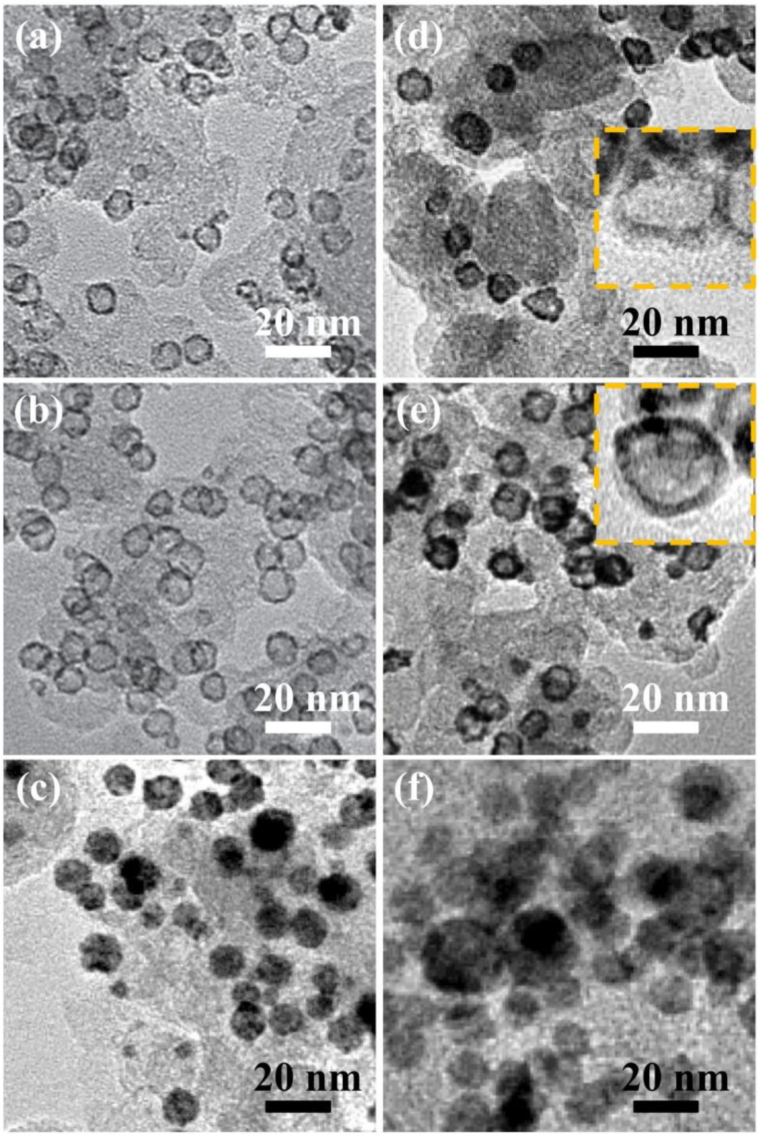

Fig. S11 Representative TEM images of (a) *r*-Pt_1Cu/C, (b) *r*-$Pt_{0.75}Cu/C$ and (c) $Pt_{0.5}Cu/C$ before and (d) *r*-Pt_1Cu/C, (e) *r*-$Pt_{0.75}Cu/C$ and (f) $Pt_{0.5}Cu/C$ after 2000 CV cycles.

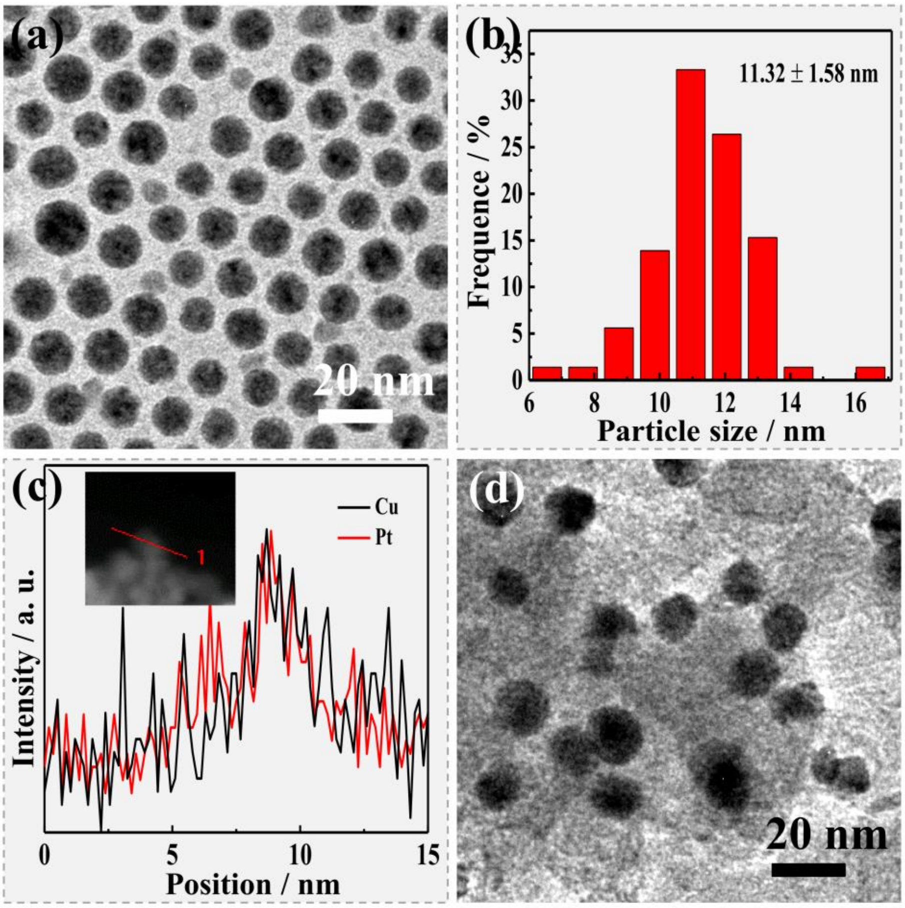

Fig. S12 (a) TEM image, (b) particle size histograms and (c) EDS line scanning profiles of the home-made solid $Pt_{0.75}Cu$ NCs; (d) TEM image of the *s*-$Pt_{0.75}Cu/C$.

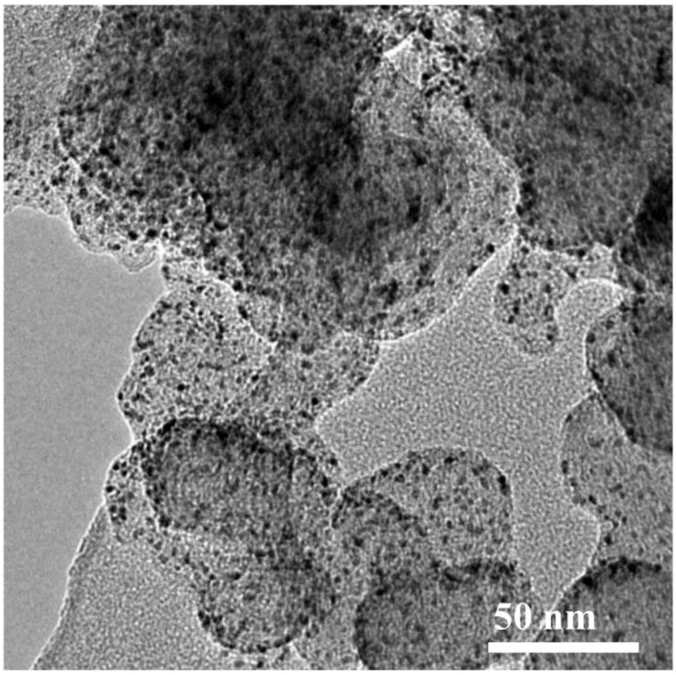

Fig. S13 TEM image of the commercial PtRu/C-JM (20 wt% Pt + 10 wt% Ru).

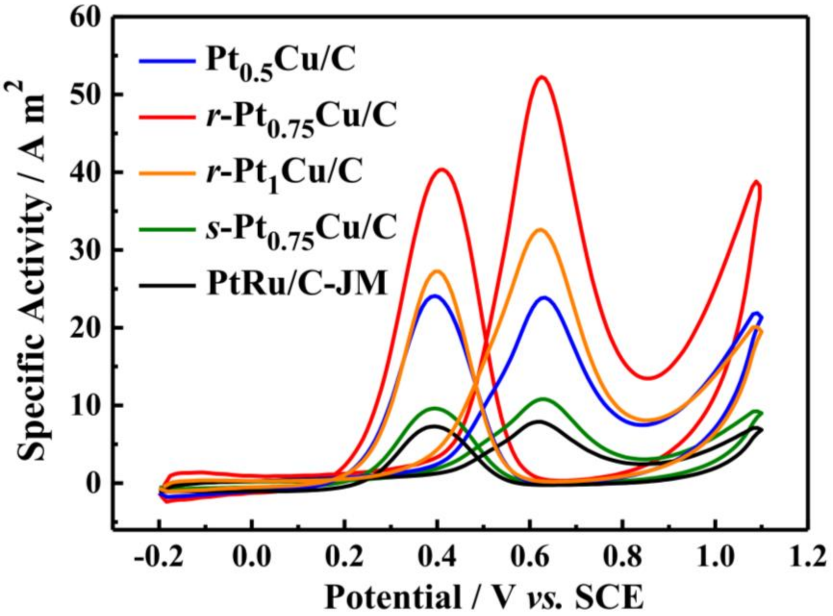

Fig. S14 Typical CVs of *r*-$Pt_{0.75}Cu/C$, *r*-Pt_1Cu/C, $Pt_{0.5}Cu/C$, *s*-$Pt_{0.75}Cu/C$ and PtRu/C-JM catalysts in N_2-saturated 0.5 M H_2SO_4 solution containing 1.0 M CH_3OH with a scan rate of 20 mV s^{-1}.

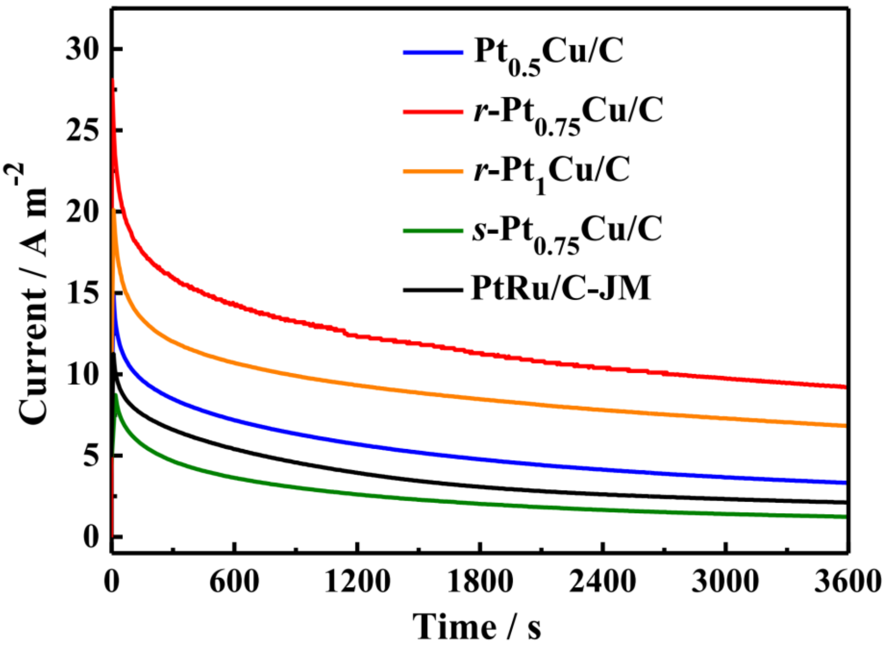

Fig. S15 CA curves of *r*-$Pt_{0.75}Cu/C$, *r*-Pt_1Cu/C, $Pt_{0.5}Cu/C$, *s*-$Pt_{0.75}Cu/C$ and PtRu/C-JM catalysts in 0.5 M H_2SO_4 solution containing 1.0 M CH_3OH at 0.6 V for 3600 s.

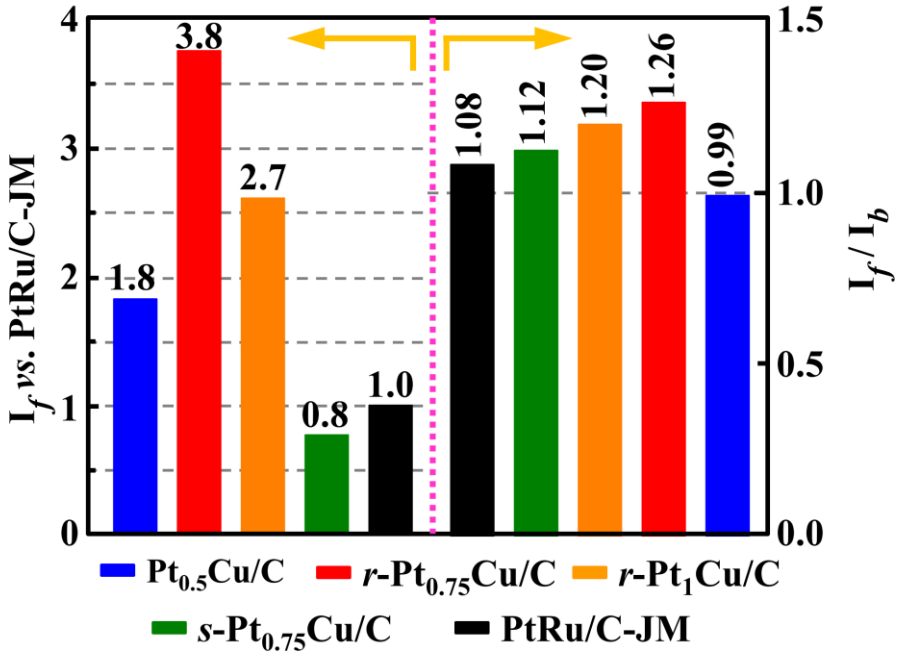

Fig. S16 Enhanced factors in mass activity for various PtCu catalysts to PtRu/C-JM, and I_f/I_b ratios of *r*-Pt$_{0.75}$Cu/C, *r*-Pt$_1$Cu/C, Pt$_{0.5}$Cu/C, *s*-Pt$_{0.75}$Cu/C and PtRu/C-JM catalysts.

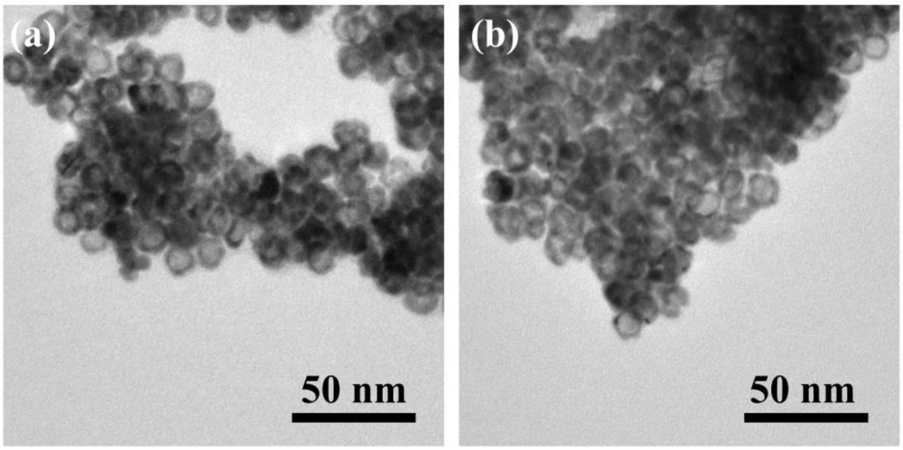

Fig. S17 TEM images of (a) $Pt_{0.75}Ir_{0.02}Cu$ NRs and (b) $Pt_{0.75}Ir_{0.1}Cu$ NRs.

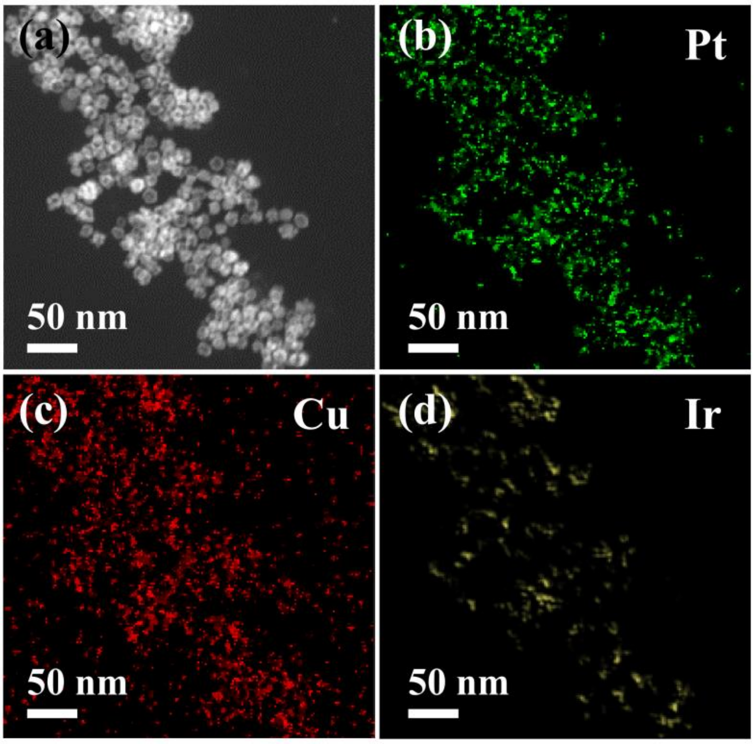

Fig. S18 (a) HAADF-STEM image of $Pt_{0.75}Ir_{0.05}Cu$ NRs and elemental mapping of (b) Pt, (c) Cu and (d) Ir.

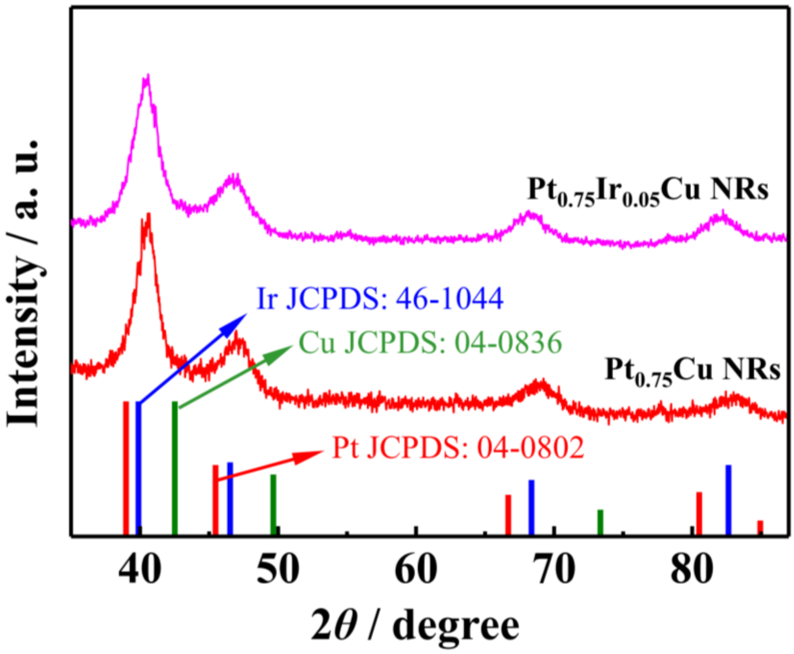

Fig. S19 PXRD patterns of $Pt_{0.75}Cu$ NRs and $Pt_{0.75}Ir_{0.05}Cu$ NRs.

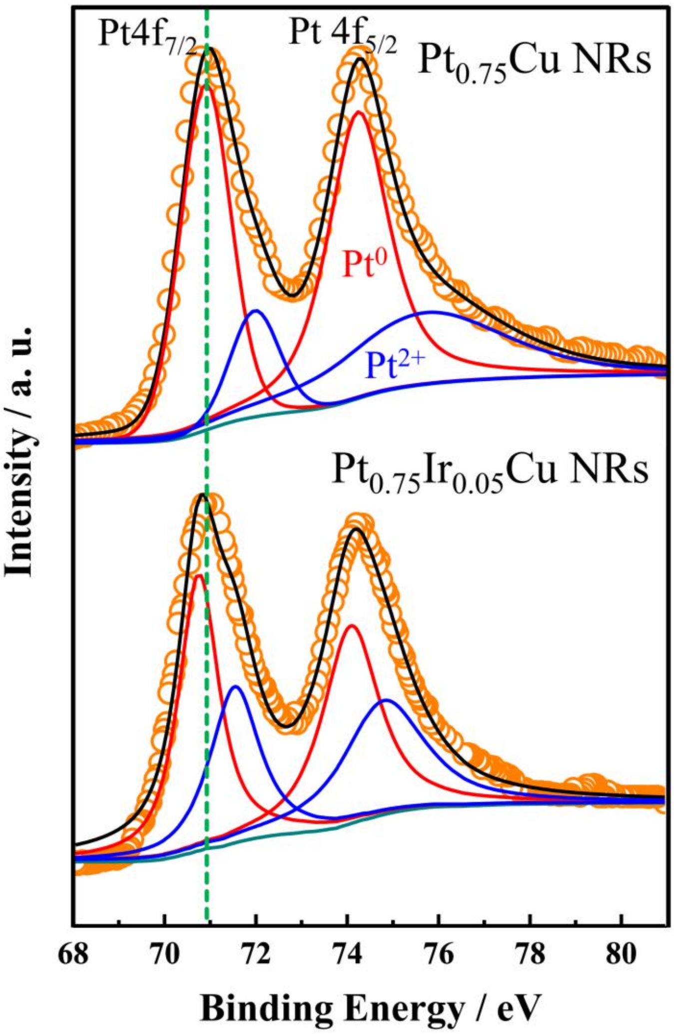

Fig. S20 XPS spectra and fitting of the Pt 4f spectral region for $Pt_{0.75}Ir_{0.05}Cu$ NRs.

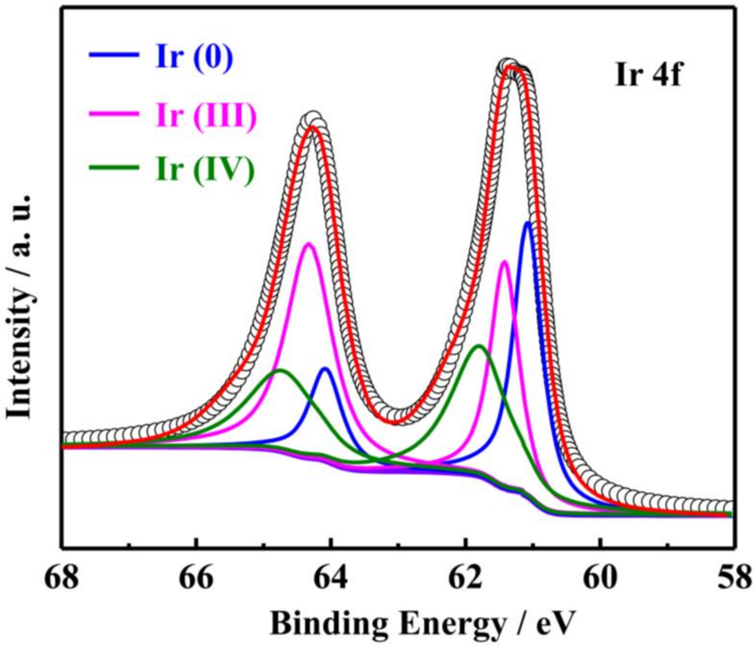

Fig. S21 XPS spectra and fitting of the Ir 4f spectral region for $Pt_{0.75}Ir_{0.05}Cu$ NRs.

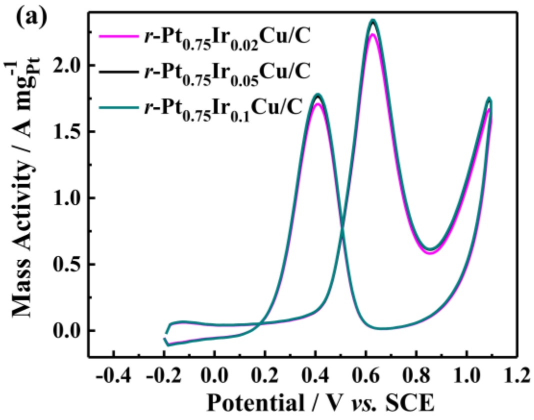

(b)

Sample	MA / A mg_{Pt}^{-1}
r-$Pt_{0.75}Ir_{0.02}Cu/C$	2.232
r-$Pt_{0.75}Ir_{0.05}Cu/C$	2.323
r-$Pt_{0.75}Ir_{0.1}Cu/C$	2.343

Fig. S22 Typical CVs of *r*-$Pt_{0.75}Ir_{0.02}Cu/C$, *r*-$Pt_{0.75}Ir_{0.05}Cu/C$ and *r*-$Pt_{0.75}Ir_{0.1}Cu/C$ in N_2-saturated 0.5 M H_2SO_4 solution containing 1.0 M CH_3OH with a scan rate of 20 mV s^{-1}.

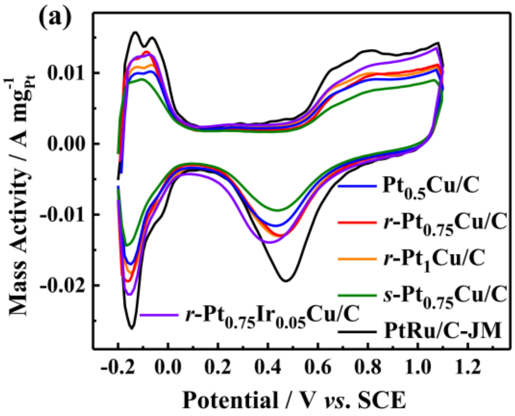

(b)

Sample	EASA / $m^2\ g_{Pt}^{-1}$
$Pt_{0.5}Cu/C$	37.15
r-$Pt_{0.75}Cu/C$	41.62
r-Pt_1Cu/C	38.86
s-$Pt_{0.75}Cu/C$	34.61
r-$Pt_{0.75}Ir_{0.05}Cu/C$	40.87
PtRu/C-JM	61.58

Fig. S23 Typical CVs of all catalysts in N_2-saturated 0.5 M H_2SO_4 solution with a scan rate of 20 mV s^{-1}.

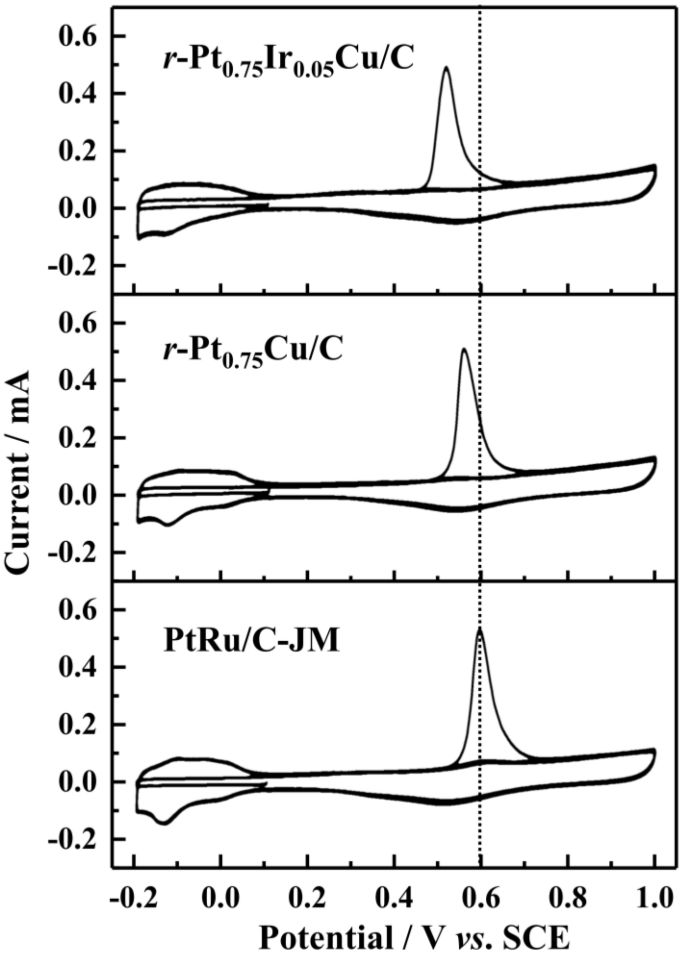

Fig. S24 CO stripping curves of PtRu/C-JM, *r*-$Pt_{0.75}Cu$/C and *r*-$Pt_{0.75}Ir_{0.05}Cu$/C in 0.5 M H_2SO_4 solution.

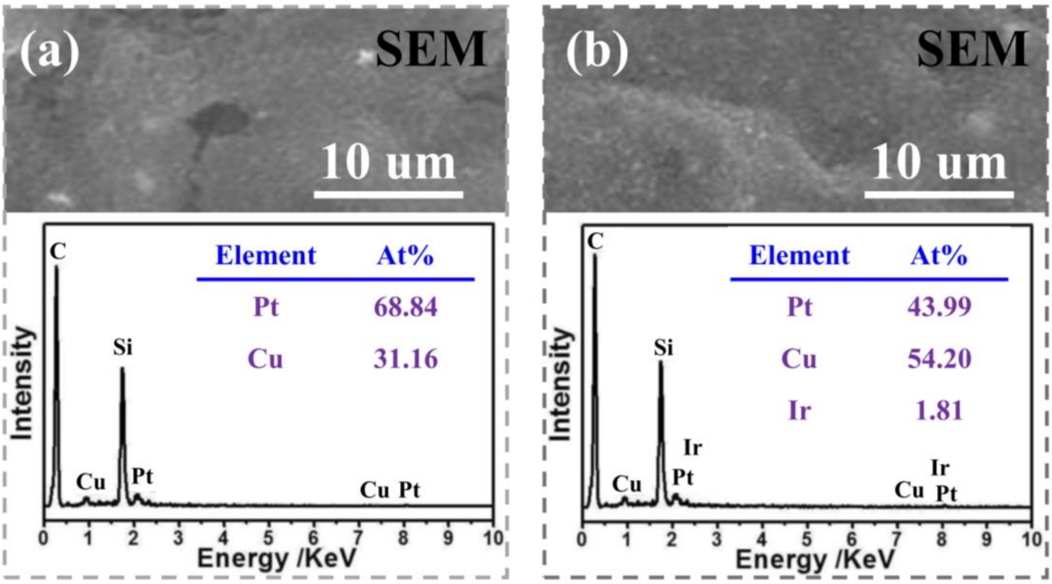

(a)

Element	At%
Pt	68.84
Cu	31.16

(b)

Element	At%
Pt	43.99
Cu	54.20
Ir	1.81

Fig. S25 SEM images and SEM-EDS spectra of (a) *r*-$Pt_{0.75}Cu/C$ and (b) *r*-$Pt_{0.75}Ir_{0.05}Cu/C$ after 10000 CV cycles. The inset table was the atomic compositions of Pt, Cu and Ir.

Supporting Tables

Table S1 Summary of the composition data for the various nanostructures on the basis of ICP-AES analysis.

Sample	Pt / w%	Cu / w%	Ir / w%	Pt / At%	Cu / At%	Ir / At%	Pt : Cu (: Ir) / At : At (: At)	
$Pt_{0.5}Cu$ NCs	61.49	38.51	/	34.21	65.79	/	34.21:65.79	0.52:1
$Pt_{0.75}Cu$ NRs	70.58	29.42	/	43.86	56.14	/	43.86:56.14	0.78:1
$Pt_{1}Cu$ NRs	76.33	23.67	/	51.22	48.78	/	51.22:48.78	1.05:1
s-$Pt_{0.75}Cu$ NCs	70.16	29.84	/	43.36	56.64	/	43.36:56.64	0.77:1
r-$Pt_{0.75}Ir_{0.1}Cu$ NRs	65.17	27.50	7.33	41.49	53.77	4.74	41.49:53.77:4.74	0.77:1:0.088
r-$Pt_{0.75}Ir_{0.05}Cu$ NRs	68.58	28.64	2.78	43.04	55.19	1.77	43.04:55.19:1.77	0.78:1:0.032
r-$Pt_{0.75}Ir_{0.02}Cu$ NRs	69.53	29.03	1.44	43.42	55.67	0.91	43.42:55.67:0.91	0.78:1:0.016

Table S2 Summary of the composition data for the products that synthesized at different reaction times on the basis of ICP-AES analysis.

Reaction time / h	Pt / w%	Cu / w%	Pt : Cu / At : At	$\frac{\text{Pt}}{\text{Pt + Cu}}$ /At%	$\frac{\text{Cu}}{\text{Pt + Cu}}$ /At%
0.5	0	100	0 : 1	0	100
1	12.74	87.26	0.048 : 1	4.58	95.42
3	51.21	48.79	0.34 : 1	29.85	70.15
6	70.58	29.42	0.78 : 1	43.86	56.14
8	64.28	35.72	0.59 : 1	37.11	62.89

Table S3 The Pt loadings, electrochemically active surface area (EASA), mass activity (MA), specific activity (SA) and I_f/i_b ratios of various catalysts in this work.

Sample	Pt / w%	EASA / $m^2\ g_{Pt}^{-1}$	MA / A mg_{Pt}^{-1}	SA / A m^{-2}	I_f/I_b
$Pt_{0.5}Cu/C$	18.7	37.15	0.887	23.88	0.99
r-$Pt_{0.75}Cu/C$	18.2	41.62	2.175	52.26	1.26
r-Pt_1Cu/C	19.2	38.86	1.267	32.60	1.20
s-$Pt_{0.75}Cu/C$	18.5	34.61	0.374	10.81	1.12
r-$Pt_{0.75}Ir_{0.05}Cu/C$	18.4	40.87	2.323	56.84	1.32
PtRu/C-JM	18.6	61.58	0.486	7.89	1.08

Table S4 The retentions in MA for *r*-$Pt_{0.75}Ir_{0.05}Cu/C$, *r*-$Pt_{0.75}Cu/C$, $Pt_{0.5}Cu/C$, *r*-Pt_1Cu/C, *s*-$Pt_{0.75}Cu/C$ and PtRu/C-JM after 500, 2000 and 10000 CV cycles.

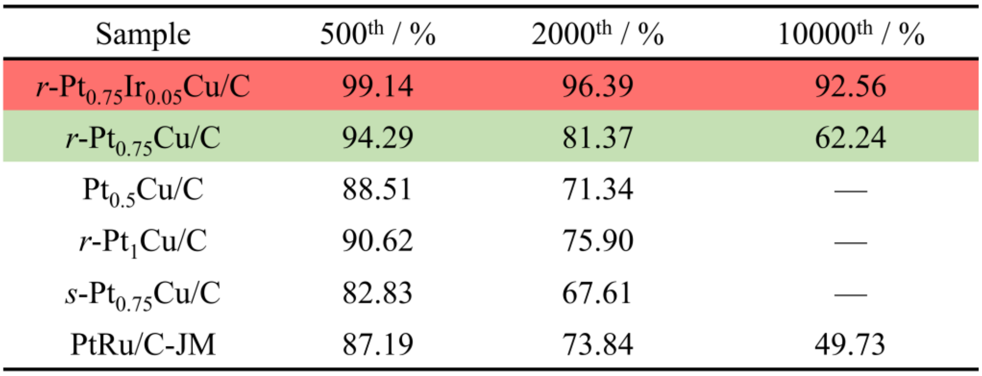

Sample	500th / %	2000th / %	10000th / %
r-$Pt_{0.75}Ir_{0.05}Cu/C$	99.14	96.39	92.56
r-$Pt_{0.75}Cu/C$	94.29	81.37	62.24
$Pt_{0.5}Cu/C$	88.51	71.34	—
r-Pt_1Cu/C	90.62	75.90	—
s-$Pt_{0.75}Cu/C$	82.83	67.61	—
PtRu/C-JM	87.19	73.84	49.73

Table S5 List of MOR activity of some PtCu nanocatalysts reported.

Catalyst	**Condition**	**MA / A mg$_{Pt}^{-1}$**	**SA / A m^{-2}**	**Ref.**
$Pt_{0.75}Cu$ nanorings	**0.5 M H_2SO_4 + 1 M CH_3OH 20 mV·s^{-1}**	**2.175**	**52.26**	**This work**
PtCu nanostars	0.5 M H_2SO_4 + 1 M CH_3OH 50 mV·s^{-1}	0.574	34.5	1
mesoporous $Pt_{84}Cu_{16}$	0.5 M H_2SO_4 + 0.5 M CH_3OH 50 mV·s^{-1}	0.314	13.9	2
PtCu nanoframes	0.5 M H_2SO_4 + 0.5 M CH_3OH 50 mV·s^{-1}	1.64	25.8	3
chain-like PtCu nanowires	0.5 M H_2SO_4 + 0.5 M CH_3OH 50 mV·s^{-1}	0.7555	25.4	4
octahedral $Pt_{34.5}Cu_{65.5}$	0.1 M H_2SO_4 + 0.5 M CH_3OH 50 mV·s^{-1}	1.43	41.2	5
Pt_1Cu_1-AA nanotubes	0.5 M H_2SO_4 + 1 M CH_3OH 50 mV·s^{-1}	2.252	60.9	6
$Pt_{55}Cu_{45}$ nanodendrites	0.1 M H_2SO_4 + 1 M CH_3OH 50 mV·s^{-1}	1.00	15.8	7
Pt_1Cu_1 nanodendrites	0.5 M H_2SO_4 + 0.5 M CH_3OH 50 mV·s^{-1}	1.4	30.1	8
$PtCu_3$ hexapods	0.5 M H_2SO_4 + 0.5 M CH_3OH 50 mV·s^{-1}	1.01	29.6	9
$PtCu_3$ nanoframes		1.861	25.5	
PtCu hexapod nanocrystals	0.5 M H_2SO_4 + 1 M CH_3OH 50 mV·s^{-1}	2.01	35.4	10
$Pt_{32}Cu_{68}$ alloy nanowires	0.5 M H_2SO_4 + 0.5 M CH_3OH 50 mV·s^{-1}	0.707	—	11
Pt_3Cu icosahedra	0.1 M $HClO_4$ + 0.2 M CH_3OH 50 mV·s^{-1}	0.746	21.7	12
dendritic Pt_3Cu cubes	0.5 M H_2SO_4 + 1 M CH_3OH 20 mV·s^{-1}	~ 0.9	—	13
PtCu nanoframes	0.1 M $HClO_4$ + 0.1 M CH_3OH 50 mV·s^{-1}	0.98	23.5	14
porous PtCu NCs	0.1 M $HClO_4$ + 1 M CH_3OH 50 mV·s^{-1}	1.55	13.01	15
Pt-Cu hierarchical branched nanoparticles	0.5 M H_2SO_4 + 1 M CH_3OH 50 mV·s^{-1}	0.635	28	16

Table S6 List of MOR activity of up-to-date Pt-based alloy nanocatalysts reported.

Catalyst	**Condition**	**MA / A mg_{Pt}^{-1}**	**SA / A m^{-2}**	**Stability**	**Ref.**
$Pt_{0.75}Ir_{0.05}Cu$ nanorings	**0.5 M H_2SO_4 + 1 M CH_3OH 20 mV·s^{-1}**	**2.323**	**56.84**	**-7.44 %, 10k cycles; -3.61 %, 2k cycles**	**This work**
$Pt_{0.75}Cu$ nanorings		**2.175**	**52.26**	**-18.63 %, 2k cycles**	
PtCo Mesoporous Nanotubes	0.5 M H_2SO_4 + 1 M CH_3OH 50 mV·s^{-1}	0.95	19.2	—	17
Pt-Ni_2P nanoparticles	0.1 M $HClO_4$ + 1 M CH_3OH 50 mV·s^{-1}	1.554	12.42	—	18
Pt@mPtRu YSs	0.5 M H_2SO_4 + 1 M CH_3OH 50 mV·s^{-1}	0.56	18.1	-16.1 %, 1k cycles	19
PtPdIr mesoporous hollow nanospheres	0.5 M H_2SO_4 + 1 M CH_3OH 50 mV·s^{-1}	1.23	19.8	-23.8 %, 1k cycles	20
Pt_3CoRu/C@NC	0.1 M $HClO_4$ + 0.5 M CH_3OH 50 mV·s^{-1}	0.97	16.0	—	21
Pt–Ni–P nanocages	0.5 M H_2SO_4 + 1 M CH_3OH 50 mV·s^{-1}	0.87	16.2	—	22
ordered PtSn/ATO	0.5 M H_2SO_4 + 1 M CH_3OH 50 mV·s^{-1}	1.52	32.8	-15 %, 0.5k cycles	23
Pt_3Zn-AA	0.5 M H_2SO_4 + 1 M CH_3OH 50 mV·s^{-1}	1.252	16.9	—	24
cross-double dumbbell-like Pt-Ni	0.5 M H_2SO_4 + 1 M CH_3OH 50 mV·s^{-1}	3.02	113	-18 %, 1k cycles	25
vertex-reinforced PtCuCo nanoframes	0.1 M $HClO_4$ + 1 M CH_3OH 50 mV·s^{-1}	4.11	133	-36.5 %, 1k cycles	26
PtRuCu hexapods	0.1 M $HClO_4$ + 1 M CH_3OH 50 mV·s^{-1}	1.35	39.1	-27 %, 0.8k cycles	27
PtRu NWs	0.1 M $HClO_4$ + 0.5 M CH_3OH 50 mV·s^{-1}	0.82	11.6	-36.33 %, 0.8k cycles	28
concave PtCo	0.1 M $HClO_4$ + 1 M CH_3OH 50 mV·s^{-1}	2.11	36.2	-31.2 %, 1k cycles	29
Worm-shaped Pt	1 M H_2SO_4 + 2 M CH_3OH 20 mV·s^{-1}	1.283	21.1	—	30
PtRu nanodendrites	0.1 M $HClO_4$ + 1 M CH_3OH 50 mV·s^{-1}	1.08	100.8	-8 %, 2k cycles	31
PtCo networks	0.1 M $HClO_4$ + 0.5 M CH_3OH 50 mV·s^{-1}	0.96	17.6	—	32
durable $Pt_{72}Ru_{28}$ porous nanoalloy	0.1 M $HClO_4$ + 0.5 M CH_3OH 50 mV·s^{-1}	1.7	—	-56.28 %, 4k cycles	33
PtNi colloidal nanocrystal clusters	0.5 M H_2SO_4 + 0.5 M CH_3OH 100 mV·s^{-1}	0.696	13.7	—	34

References

1. L. Huang, W. Zhang, P. Li, Y. Song, H. Sheng, Y. Du, Y. G. Wang, Y. Wu, X. Hong, Y. Ding, X. Yuan and M. Zhu, *Nano Res.*, 2019, **12**, 1147-1153.
2. Y. Kang, B. Jiang, Z. A. Alothman, A. Y. Badjah, M. Naushad, M. Habila, S. Wabaidur, J. Henzie, H. Li and Y. Yamauchi, *Chem.*, 2019, **25**, 343-348.
3. X. Li, Y. Zhou, Y. Du, J. Xu, W. Wang, Z. Chen and J. Cao, *Int. J. Hydrogen Energy*, 2019, **44**, 18050-18057.
4. J. Cao, Y. Du, M. Dong, Z. Chen and J. Xu, *J. Alloys and Compd.*, 2018, **747**, 124-130.
5. Chaozhong Li, T. Liu, T. He, B. Ni, Q. Yuan and X. Wang, *Nanoscale*, 2018, **10**, 4670-4674.
6. H. H. Li, Q. Q. Fu, L. Xu, S. Y. Ma, Y. R. Zheng, X. J. Liu and S. H. Yu, *Energy Environ. Sci.*, 2017, **10**, 1751-1756.
7. L. Guo, L. Huang, W. Jiang, Z. Wei, L. Wan and J. Hu, *J. Mater. Chem. A*, 2017, **5**, 9014-9021.
8. L. Lu, S. Chen, S. Thota, X. Wang, Y. Wang, S. Zou, J. Fan and J. Zhao, *J. Phys. Chem. C*, 2017, **121**, 19796-19806.
9. Y. L. Xiong, Y. L. Ma, Z. Q. Lin, Q. F. Xu, Y. C. Yan, H. Zhang, J. B. Wu and D. Yang, *CrystEngComm*, 2016, **18**, 7823-7830
10. K. Wang, R. Sriphathoorat, S. Luo, M. Tang, H. Du and P. K. Shen, *J. Mater. Chem. A*, 2016, **4**, 13425-13430.
11. Y. Liao, G. Yu, Y. Zhang, T. Guo, F. Chang and C. J. Zhong, *J. Phys. Chem. C*, 2016, **120**, 10476-10484.
12. X. H. Sun, K. Z. Jiang, N. Zhang, S. J. Guo and X. Q. Huang, *ACS Nano*, 2015, **9**, 7634-7640.
13. Y. Kuang, Y. Zhang, Z. Cai, G. Feng, Y. Jiang, C. Jin, J. Luo and X. Sun, *Chem. Sci.*, 2015, **6**, 7122-7129.
14. J. Ding, X. Zhu, L. Bu, J. Yao, J. Guo, S. Guo and X. Huang, *Chem. Commun.*, 2015, **51**, 9722-9725.
15. K. Eid, H. Wang, P. He, K. Wang, T. Ahamad, S. M. Alshehri, Y. Yamauchi and L. Wang, *Nanoscale*, 2015, **7**, 16860-16866.
16. Y. Cao, Y. Yang, Y. Shan and Z. Huang, *ACS Appl. Mater. Interfaces*, 2016, **8**, 5998-6003.
17. S. Yin, Z. Wang, X. Qian, D. Yang, Y. Xu, X. Li, L. Wang and H. Wang, *ACS Sustain. Chem. Eng.*, 2019, **7**, 7960-7968.
18. H. Liu, D. Yang, Y. Bao, X. Yu and L. Feng, *J. Power Sources*, 2019, **434**, 226754.

19. S. Yin, R. D. Kumar, H. Yu, C. Li, Z. Wang, Y. Xu, X. Li, L. Wang and H. Wang, *ACS Sustain. Chem. Eng.*, 2019, **7**, 14867-14873.
20. K. Deng, Y. Xu, Z. Dai, H. Yu, S. Yin, Z. Wang, X. Li, L. Wang and H. Wang, *Chem. Asian J.*, 2019, **14**, 3868-3874.
21. Q. Wang, S. Chen, H. Lan, P. Li, X. Ping, S. Ibraheem, D. Long, Y. Duan and Z. Wei, *J. Mater. Chem. A*, 2019, **7**, 18143-18149.
22. K. Deng, Y. Xu, D. Yang, X. Qian, Z. Dai, Z. Wang, X. Li, L. Wang and H. Wang, *J. Mater. Chem. A*, 2019, **7**, 9791-9797.
23. W. Chen, Z. Lei, T. Zeng, L. Wang, N. Cheng, Y. Tan and S. Mu, *Nanoscale*, 2019, **11**, 19895-19902.
24. X. Zhang, I. G. A. Ossufo, H. Ye, Y. Huang, S. Ge, Z. Xiang, Y. Cui and R. Wang, *ChemCatChem*, 2019, DOI: 10.1002/cctc.201900649.
25. W. Gong, Z. Jiang, R. Wu, Y. Liu, L. Huang, N. Hu, P. Tsiakaras and P. K. Shen, *Appl. Catal. B: Environ.*, 2019, **246**, 277-283.
26. T. Kwon, M. Jun, H. Y. Kim, A. Oh, J. Park, H. Baik, S. H. Joo and K. Lee, *Adv. Funct. Mater.*, 2018, **28**,1706440.
27. S. Xue, W. Deng, F. Yang, J. Yang, I. S. Amiinu, D. He, H. Tang and S. Mu, *ACS Catal.*, 2018, **8**, 7578-7584.
28. L. Huang, X. Zhang, Q. Wang, Y. Han, Y. Fang and S. Dong, *J. Am. Chem. Soc.*, 2018, **140**, 1142-1147.
29. Y. Ma, L. Yin, T. Yang, Q. Huang, M. He, H. Zhao, D. Zhang, M. Wang and Z. Tong, *ACS Appl. Mater. Interfaces*, 2017, **9**, 36164-36172.
30. H. Huang, L. Ma, C. S. Tiwary, Q. Jiang, K. Yin, W. Zhou and P. M. Ajayan, *Small*, 2017, **13**, 1603013.
31. S. Lu, K. Eid, D. Ge, J. Guo, L. Wang, H. Wang and H. Gu, *Nanoscale*, 2017, **9**, 1033-1039.
32. J. Ding, S. Ji, H. Wang, B. G. Pollet and R. Wang, *Electrochim. Acta*, 2017, **255**, 55-62.
33. W. Y. Zhao, B. Ni, Q. Yuan, P. L. He, Y. Gong, L. Gu and X. Wang, *Adv. Energy Mater.*, 2017, **7**, 1601593.
34. P. Yang, X. Yuan, H. Hu, Y. Liu, H. Zheng, D. Yang, L. Chen, M. Cao, Y. Xu, Y. Min, Y. Li and Q. Zhang, *Adv. Funct. Mater.*, 2018, **28**, 1870001.